Journal of Applied Geophysics 114 (2015) 116–122

Contents lists available at ScienceDirect

Journal of Applied Geophysics

journal homepage: www.elsevier.com/locate/jappgeo

An efficient discontinuous Galerkin finite element method with nested domain decomposition for simulations of microresistivity imaging

Jiefu Chen

Advantage R&D Center, Weatherford, Houston, TX 77060, USA

ARTICLE INFO

Article history:
Received 17 November 2014
Accepted 9 January 2015
Available online 17 January 2015

Keywords:
Well logging
Microresistivity imaging
Discontinuous Galerkin finite element method (DG-FEM)
Domain decomposition
Block Thomas method

ABSTRACT

A discontinuous Galerkin finite element method is employed to study the responses of microresistivity imaging tools used in the oil and gas exploration industry. The multiscale structure of an imaging problem is decomposed into several nested subdomains based on its geometric characteristics. Each subdomain is discretized independently, and numerical flux is used to couple all subdomains together. The nested domain decomposition scheme will lead to a block tridiagonal linear system, and the block Thomas algorithm is utilized here to eliminate the subdomain based iteration in the step of solving the linear system. Numerical results demonstrate the validity and efficiency of this method.

1. Introduction

Microresistivity imaging (Luthi, 2001) tools are very useful in oilfield services. For the logging-while-drilling (LWD) type of micro-resistivity tool, an imaging pad containing a button electrode as the receiving sensor is mounted on the bottom hole assembly (Haramboure and Wisler, 2013). Two nonconductor pipes are attached to the two ends of the imaging pad to make it isolated from the drilling collar, which is made of steel. The button electrode is also isolated from the pad by an insulating ring. When this tool is working, a certain oscillating potential is applied onto the pad (including the button electrode) to excite a focused field and make currents flow from the tool into the formation, and the button electrode is used to measure currents that flow through it, which changes with the variation of the formation resistivity. As the drill bit progresses, the button electrode makes a full coverage of the borehole wall, and correspondingly generates a high resolution image of resistivity distribution, such as the one shown in the left panel of Fig. 1. Microresistivity imaging tools are capable of unveiling very detailed subsurface structures such as fractures, vugs, bed interfaces, and faults, which are very important in oil and gas drilling and production. An accurate and efficient simulation of the microresistivity imaging tool working in complex environments is critical to tool design as well as field data interpretation.

Modeling microresistivity imaging is oftentimes a multiscale problem. As shown in the right panel of Fig. 1, the length of an imaging tool is a few meters, the lengths of imaging pad and two insulators are around tens of centimeters, the diameter of the button electrode is about one centimeter, and details on the borehole wall such as fractures can be as small as several millimeters or even micrometers. This multiscale property will raise severe challenges for conventional numerical methods. Take the popular finite element method (FEM) (Coggon, 1971; Brezzi et al., 1985; Wang, 2000) for instance: extremely small elements are needed to capture geometric details of small fractures and imaging sensors, while relatively big elements should be used to discretize the remaining large bulk of formation. FEM uses one globally conforming mesh, which means a transition of discretization density is required from very small elements to fairly large elements. A gradual mesh transition will inevitably lead to unnecessary dense mesh and unknowns for electrically large structures, and a prohibitively expensive system of equations to solve. On the other hand, an abrupt transition from dense mesh to coarse mesh may save some unknowns, but it will greatly increase the meshing difficulty as well as condition number of the discretized system, leading to a very slow convergence or even non-convergence in solving the discretized FEM system.

In this study we employ the discontinuous Galerkin finite element method (DG-FEM) (Arnold et al., 2002; Lu et al., 2005; Hesthaven and Warburton, 2008; Chen et al., 2010; Chen and Liu, 2013) with nested domain decomposition to solve this multiscale problem. The whole structure is divided into several subdomains in a nested way: small and lower order finite elements are used to capture geometric characteristics of fine structures such as imaging sensors and fractures on the borehole wall; large and higher order finite elements are used to efficiently discretize electrically coarse structures. Subdomains are discretized independently. The numerical flux, or the DG operator, is utilized to stitch all subdomains together. A discretized system by the DG-FEM method is usually solved by subdomain based iterative

E-mail address: jiefu.chen@weatherford.com.

http://dx.doi.org/10.1016/j.jappgeo.2015.01.006
0926-9851/

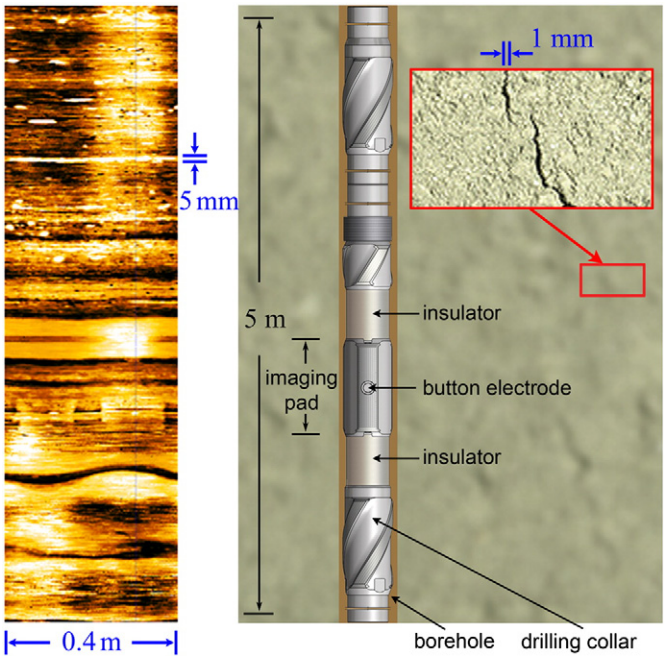

Fig. 1. Left: a typical microresistivity image with recognizable patterns of fractures, vugs, bed interfaces, etc.; Right: schematic of a microresistivity tool in formation with fine details.

algorithm, such as the block Gauss–Seidel method (Tavakoli and Davami, 2007), whose convergence rate is determined by convergence threshold, total number of subdomains, and the condition number of each discretized matrix equation. Here we propose a nested domain decomposition strategy suited to structures of microresistivity imaging problems. A nested domain decomposition will lead to a block tridiagonal linear system, and can use the block Thomas method (Meurant, 1992; Chen et al., 2011), an iteration free algorithm, to solve the system of matrix equations. We show several examples by both the conventional FEM and the proposed DG-FEM in the end of this paper. Good agreements are observed between the two methods, and the proposed DG-FEM scheme is demonstrated to be more efficient than the conventional FEM in modeling the multiscale microresistivity imaging problems.

2. Governing equations and discontinuous Galerkin weak forms

The micro-resistivity measurement can be in time domain or in frequency domain. Here we consider the application of imaging tool in water based mud, where the resistivity of drilling fluid is relatively low and electric current conduction is the dominating phenomenon while imaging. Micro-resistivity imaging in this situation is oftentimes in the range of around 1 kHz to 10 kHz, and such a low frequency leads to a quasi-static physics.

To use DG-FEM to solve the quasi-static micro-imaging problem, we need to write the governing equations as a set of first order partial differential equations with current density $\mathbf{J}$ and electric potential Φ as variables

$$\nabla \cdot \mathbf{J} = 0 \tag{1}$$

$$\mathbf{J} + (\sigma + j\omega\epsilon)\nabla\Phi = \mathbf{J}_e \tag{2}$$

where ω is the working frequency of the imaging tool, and $\mathbf{J}_e$ is the external current density. ϵ is material's permittivity, and σ denotes conductivity, which is the inverse of electrical resistivity.

Denote scalar N_ϕ as basis function for electric potential Φ as well as testing function for Eq. (1), and vector $\mathbf{N}_j$ as basis function for current density $\mathbf{J}$ as well as testing function for Eq. (2). The Galerkin's weak forms of the above governing equations are

$$\int_V N_\phi \nabla \cdot \mathbf{J} dV = 0 \tag{3}$$

$$\int_V \mathbf{N}_j \cdot (\mathbf{J} + (\sigma + j\omega\epsilon)\nabla\Phi) dV = \int_V \mathbf{N}_j \cdot \mathbf{J}_e dV \tag{4}$$

where V denotes the volume for integration. With integration by parts, Eqs. (3) and (4) will be changed as

$$\int_V \nabla N_\phi \cdot \mathbf{J} dV - \int_S N_\phi \hat{\mathbf{n}} \cdot \mathbf{J} dS = 0 \tag{5}$$

$$\int_V \mathbf{N}_j \cdot \mathbf{J} dV - \int_V (\sigma + j\omega\epsilon)\left(\nabla \cdot \mathbf{N}_j\right)\Phi dV + \int_S (\sigma + j\omega\epsilon)\left(\hat{\mathbf{n}} \cdot \mathbf{N}_j\right)\Phi dS = \int_V \mathbf{N}_j \cdot \mathbf{J}_e dV \tag{6}$$

where S denotes the surface, and $\hat{\mathbf{n}}$ is the unit normal vector located on S and pointing to the outside of V.

The surface integration items in Eqs. (5) and (6) are determined by either boundary conditions (for boundaries) or numerical fluxes (for interfaces between subdomains). Assuming the k-th and the l-th subdomains as the local subdomain and its neighbor, respectively, the interface evaluations of $\hat{\mathbf{n}} \cdot \mathbf{J}$ and Φ are determined by the field values of subdomains on both sides

$$\hat{\mathbf{n}} \cdot \mathbf{J} = \frac{1}{2}\left(\hat{\mathbf{n}} \cdot \mathbf{J}^{(k)} + \hat{\mathbf{n}} \cdot \mathbf{J}^{(l)}\right) + C_{11}\left(\hat{\mathbf{n}} \cdot \mathbf{J}^{(k)} - \hat{\mathbf{n}} \cdot \mathbf{J}^{(l)}\right) + C_{12}\left(\Phi^{(k)} - \Phi^{(l)}\right) \tag{7}$$

and

$$\Phi = \frac{1}{2}\left(\Phi^{(k)} + \Phi^{(l)}\right) + C_{21}\left(\hat{\mathbf{n}} \cdot \mathbf{J}^{(k)} - \hat{\mathbf{n}} \cdot \mathbf{J}^{(l)}\right) + C_{22}\left(\Phi^{(k)} - \Phi^{(l)}\right) \tag{8}$$

where coefficients C_{11}, C_{12}, C_{21}, and C_{22} can have different choices. By adjusting the values of those coefficients, we can obtain different DG-FEM schemes with their own numerical features (Li, 2006). For example, in the following two examples we set the coefficients as $C_{11} = -0.5$, $C_{12} = -4$, $C_{21} = 0$, and $C_{22} = 0.5$, and this combination is corresponding to an upwind flux.

3. DG-FEM discretization

Assuming a microresistivity imaging problem is divided into N subdomains, the discretized system by DG-FEM will be a set of matrix equations

$$\mathbf{K}_{\phi j}^{(k)} \mathbf{j}^{(k)} + \sum_{l=1}^{N}\left(\mathbf{L}_{\phi\phi}^{(kl)} \phi^{(l)} + \mathbf{L}_{\phi j}^{(kl)} \mathbf{j}^{(l)}\right) = 0 \tag{9}$$

and

$$\mathbf{M}_{jj}^{(k)} \mathbf{j}^{(k)} + \mathbf{K}_{j\phi}^{(k)} \phi^{(k)} + \sum_{l=1}^{N}\left(\mathbf{L}_{j\phi}^{(kl)} \phi^{(l)} + \mathbf{L}_{jj}^{(kl)} \mathbf{j}^{(l)}\right) = \mathbf{j}_e^{(k)} \tag{10}$$

where $k = 1, 2, \cdots N$. $\phi^{(k)}$ and $\mathbf{j}^{(k)}$ are vectors of discretized electric potential and current density, and $\mathbf{j}_e^{(k)}$ is vector of discretized external excitation. $\mathbf{M}_{jj}^{(k)}$, $\mathbf{K}_{\phi j}^{(k)}$, and $\mathbf{K}_{j\phi}^{(k)}$ are mass and stiffness matrices of the k-th subdomain. Matrices $\mathbf{L}_{\phi\phi}^{(kl)}$, $\mathbf{L}_{\phi j}^{(kl)}$, $\mathbf{L}_{j\phi}^{(kl)}$, and $\mathbf{L}_{jj}^{(kl)}$ are obtained from the interface integrations and can be viewed as